Estimating the parameter sensitivity of acoustic mode quantities for an idealized shelf-slope front

Brendan J. DeCourcy, Ying-Tsong Lin, and William L. Siegmann

Citation: The Journal of the Acoustical Society of America **143**, 706 (2018); doi: 10.1121/1.5022776
View online: https://doi.org/10.1121/1.5022776
View Table of Contents: http://asa.scitation.org/toc/jas/143/2
Published by the Acoustical Society of America

Estimating the parameter sensitivity of acoustic mode quantities for an idealized shelf-slope front

Brendan J. DeCourcy,[1,a)] Ying-Tsong Lin,[2] and William L. Siegmann[1]
[1]*Department of Mathematical Sciences, Rensselaer Polytechnic Institute, Troy, New York 12180, USA*
[2]*Applied Ocean Physics and Engineering Department, Woods Hole Oceanographic Institution, Woods Hole, Massachusetts 02543, USA*

(Received 29 August 2017; revised 9 January 2018; accepted 12 January 2018; published online 6 February 2018)

The acoustic modes of an idealized three-dimensional model for a curved shelf-slope ocean front [Lin and Lynch, J. Acoust. Soc. Am. **131**, EL1–EL7 (2012)] is examined analytically and numerically. The goal is to quantify the influence of environmental and acoustic parameters on acoustic field metrics. This goal is achieved by using conserved quantities of the model, including the dispersion relation and a conservation of mode number. Analytic expressions for the horizontal wave numbers can be extracted by asymptotic approximations and perturbations, leading to accurate and convenient approximations for their parameter dependence. These equations provide the dependence on model parameter changes of both the real horizontal wavenumbers, leading to modal phase speeds and other metrics, and the imaginary parts, leading to modal attenuation coefficients. Further approximations for small parameter changes of these equations characterize the parameter sensitivities and produce assessments of environmental and acoustic influences.
 https://doi.org/10.1121/1.5022776

[JFL] Pages: 706–715

I. INTRODUCTION

Sound propagation near ocean fronts on the sloping continental shelf has been studied extensively, including the PRIMER experiments in the Mid-Atlantic Bight,[1,2] the SW'06 experiments off the New Jersey coast,[3,4] and the Barents Sea Polar Front.[5] Curved fronts are known to influence acoustic propagation, and there is particular interest in the extent to which frontal environmental and acoustic parameters contribute to this effect. Curved 3-D front environments such as the shelf-slope front[6,7] or shallow water ducting by curved nonlinear internal waves[8,9] have been treated analytically using ocean feature models, as well as computationally. The importance of data uncertainty is examined by Jiang *et al*. in the context of analyzing data collected along the New Jersey Shelf.[10] When 3-D computational models of real ocean environments are employed for acoustic propagation applications such as in the Integrated Ocean Dynamics and Acoustics (IODA) project,[11,12] estimates should be obtained for how much the ocean feature variability affects acoustic predictions. Our premise is that parameter variations in idealized 3-D feature models generically correspond to the variability introduced into computational ocean model results, and consequently to a portion of the uncertainty in observational data. Specifying the effects of parameter variations on acoustic metrics, such as transmission loss, modal wavenumbers, modal attenuations, and modal cycle distances, is an important step toward identifying uncertainty in computational predictions of 3-D ocean acoustic propagation. In this paper, convenient formulas for the dependence of feature model parameters in the idealized 3-D shelf-slope front of Ref. 6 are obtained and used to determine their influence on acoustic quantities.

The primary approach by which these sensitivity equations are found is through conserved, or nearly conserved, normal mode quantities. The latter are so effective because they involve most or all of the model parameters, and specifically they include the implicit parameter dependence for modal wavenumbers. The extraction of parameter dependence from ocean waveguides has been performed previously, leading to linear approximations for small parameter changes.[13] Early papers by Weston[14] and by Pierce[15] for adiabatic environments developed waveguide invariants for rays and normal modes. Requirements for using the adiabatic approximation were formulated by Milder,[16] Brekhovskikh and Lysanov,[17] and Colosi,[18] and typically these requirements need to be considered with a coastal front model or a sloping bottom.[19,20] However, the choice of front representation, ocean boundaries, and coordinate system for the idealized front model of Lin and Lynch[6] described in Sec. II eliminates coupling terms in the normal mode solution. As a result, the mode number invariance derived in Refs. 14 and 15 is the most effective starting point for calculating parameter dependence for the curved shelf-slope front model. In Sec. VI, nonlinear expressions for horizontal wavenumbers will be found to provide accurate dependence over wide intervals of parameter values.[21] In Sec. VII, local parameter approximations will be calculated to show conveniently the sensitivity behavior.

II. THE IDEALIZED FRONT SOLUTION METHOD AND CLASSIFICATION OF RADIAL MODES

The idealized coastal shelf front model is the same as in Refs. 6 and 7 and is sketched in Fig. 1(a). Cylindrical coordinates are (r, θ, y), the y-axis is the shoreline, and θ is the

[a)]Electronic mail: decoub@rpi.edu

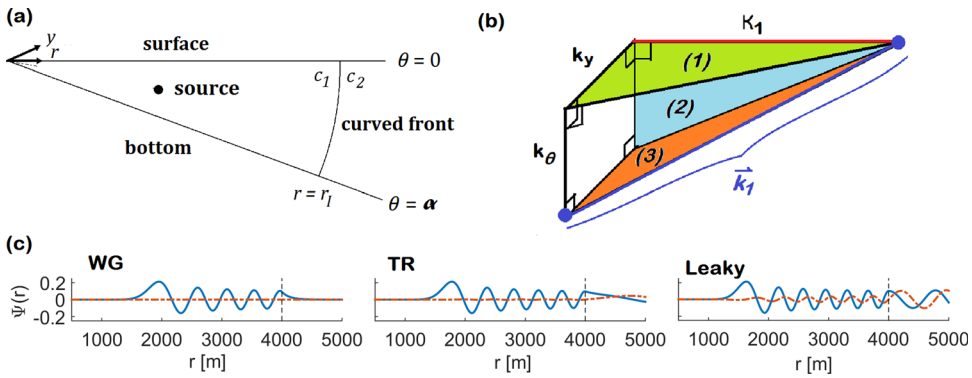

FIG. 1. (Color online) Idealized shelf-slope front model in cylindrical coordinates (r, θ, y). Parameters are front location $r = r_I$, source frequency f, inshore/offshore sound speeds c_1/c_2, bottom slope angle α. Boundary conditions are pressure release at $\theta = 0$ and perfectly reflecting at $\theta = \alpha$. (b) Schematic of prism with three numbered faces that show components $(k_y, k_\theta, \kappa_1)$ of the inshore medium wavenumber vector $\vec{k}_1$. (c) Sketches of real parts (solid, blue) and imaginary parts (dashed, red) versus radial distance r of the radial mode types: Whispering gallery (WG), transition (TR), and leaky for the front model.

angle from the horizontal surface $\theta = 0$. The curved front is modeled by a sound speed jump at $r = r_I$, with sound speed c_1 inshore $(r < r_I)$ and c_2 offshore $(r > r_I)$. The coastal ocean wedge has a constant bottom slope angle α, with a pressure release surface and perfectly reflecting bottom. In this paper the reference parameter values used for numerical examples are[6,7] $r_I = 4000$ m, $\alpha = 3°$, $f = 25$ Hz, $c_1 = 1500$ m/s, $c_2 = 1520$ m/s.

Lin and Lynch provide a solution for acoustic pressure $P(r, \theta, y)e^{-i\omega t}$ from a point source at $(r_0, \theta_0, 0)$ and frequency ω where P satisfies the Helmholtz equation

$$(\nabla^2 + k^2(r))P(r,\theta,y) = -4\pi\frac{\delta(r-r_0)}{r}\delta(\theta-\theta_0)\delta(y). \quad (1)$$

The wavenumber is $k(r) = k_j$ with $j = 1$ inshore, $j = 2$ offshore, and $k_j = 2\pi f/c_j$. A Fourier transform in y is applied to Eq. (1) to obtain an equation for $\hat{P}(r, \theta, k_y)$, where k_y is referred to as the horizontal wavenumber. The expression for $\hat{P}$ is obtained in Refs. 6 and 7, by expanding in a series of angular and radial normal modes of the homogeneous Eq. (1). The sloping bottom suggests that mode coupling might occur in the solution. Examples of coupled modes in a coastal wedge are described by Arnold[22] and Hall,[23] and an assessment of their importance for a coastal shelf is given by Knobles *et al.*[24] However, in the idealized front here, no cross terms arise from substituting a modal expansion for $\hat{P}$ and using orthogonality. The coordinate geometry of the front model means that the adiabatic approximation is valid,[15] and can be perturbed to investigate mode coupling.[25]

The solution for P requires a complex inversion of $\hat{P}(r, \theta, k_y)$. Then P can be represented by a sum of residues and a branch line integral in the complex k_y plane. The latter is evaluated using a Pekeris cut, with the relevant branch lines emanating from k_j to $k_j + i\infty$. The branch line integral is an important solution contributor for small y; for larger y the sum of improper modes revealed as residues by the Pekeris cut approximates the solution[13,26] sufficiently well.[13,27]

Neglecting the branch line integral, P is approximately[6]

$$P(r,\theta,y) \approx \sum_n\sum_m Q_{nm}\Phi_n(\theta_0)\Psi_{nm}(r_0, k_{y,nm})\Phi_n(\theta) \times \Psi_{nm}(r, k_{y,nm})e^{ik_{y,nm}y}, \quad (2)$$

where the radial modes Ψ_{nm} are given by combinations of Bessel and Hankel functions,[6,7] and the angular modes are $\Phi_n(\theta) = (\sqrt{2/\alpha\pi})\sin(\eta_n\theta)$. The integers n and m are angular and radial mode numbers. The quantities $k_{rj,nm} = \sqrt{k_j^2 - k_y^2}$ are wavenumbers that describe wavefront propagation in any vertical (r, θ) plane. The quantity $\eta_n = (\pi/\alpha)(n - 1/2)$ is a dimensionless angular wavenumber. The modal weight coefficient Q_{nm} is expressed in Ref. 6 in terms of the residue at pole nm in $\hat{P}$. Integers m and n will be omitted in subsequent formulas except where essential.

Modal behavior in the idealized front model is an important consideration in analyzing parameter sensitivity. For example, radial modes exhibit behaviors that classify them as trapped, leaky, or "transition." It is useful to quantify the properties of each radial mode type, as well as the parameter conditions for which a radial mode may undergo a type change. The simplest specification of mode types is based on radial wavenumbers κ_{rj}, where

$$\kappa_{rj}(r) = \sqrt{k_j^2 - k_y^2 - \frac{\eta^2}{r^2}}. \quad (3)$$

The κ_{rj} appear in the radial mode equation[6]

$$\frac{1}{r}\frac{d}{dr}\left(r\frac{d\Psi}{dr}\right) + \kappa_{rj}(r)^2\Psi = 0, \quad j = 1, 2. \quad (4)$$

If the sign of the squared radial wavenumber κ_{rj}^2 is positive (or negative), the radial mode behavior is oscillatory (or exponential). Note that the wavenumber in the water (k_j) is expressed in terms of the horizontal, radial, and angular wavenumbers by the equation

$$k_j^2 = k_y^2 + \kappa_{rj}^2(r) + \frac{\eta^2}{r^2}. \quad (5)$$

Figure 1(b) is a prism constructed from wavenumber components, with face (1) from radial and horizontal wavenumbers, face (2) from radial and angular components, and face (3) from horizontal and angular components.

Because $\kappa_{rj}^2 = 0$ provides the condition for a change (or turning point) between oscillatory and exponential radial mode behaviors, there are corresponding conditions on k_y for both regions $j = 1$ and 2. If in Eq. (3) $k_y = k_j^*$, where

$$k_j^* = \sqrt{k_j^2 - \frac{\eta^2}{r^2}}, \tag{6}$$

then the r-dependent radial wavenumber $\kappa_{rj} = 0$. First, let k_j^* be evaluated at $r = r_I$ to examine radial mode behavior near the front. Let $\mathrm{Re}(k_y) < k_1^*$; then oscillations will occur inshore near the front, meaning a radial mode may exist. If $\mathrm{Re}(k_y) > k_2$, then from Eq. (3) with $j = 2$, no oscillations occur offshore. Therefore, a k_y value satisfying $k_2 < \mathrm{Re}(k_y) < k_1^*$ is a trapped or whispering gallery (WG) mode as illustrated in the first panel of Fig. 1(c). Next, if $\mathrm{Re}(k_y) < k_2^*$, then from Eq. (3) with $j = 2$, oscillatory behavior occurs offshore, so such modes satisfy requirements for a leaky mode as shown in the third panel of Fig. 1(c). Finally, transition modes (TR) are those with $k_2^* < \mathrm{Re}(k_y) < k_2$. Transition modes are unusual in that they are not trapped, but the range dependence of the dimensional azimuthal wavenumber $\eta/r = k_\theta$ in Eq. (3) prevents $\mathrm{Re}(\kappa_{r2}(r))$ from being positive close to the front. This results in weaker energy transmission across the front compared to leaky modes, and oscillations for large r in contrast with WG modes. Note that it is possible for parameter combinations to produce $k_1^* < k_2$, implying no WG modes, although this does not occur for the reference parameters here.

III. PLANE-WAVE APPROXIMATION FOR CALCULATING AN OCEAN-WEDGE INVARIANT QUANTITY

An important step towards specifying parameter dependence for the idealized front model is to identify conserved quantities of the normal mode pressure solution. For adiabatic propagation in a 2-D ocean, Weston[14] derived an integral quantity conserving (vertical) mode number

$$\int_0^H k \, \sin\phi \, dZ = \pi M - \frac{1}{2}(\Theta_B + \Theta_S). \tag{7}$$

The quantity k is a local wavenumber, ϕ is the ray path angle with the horizontal, and Z is depth. Depth of the waveguide is H, 0 denotes the top, and Θ_B and Θ_S describe phase changes at the bottom and surface. In Eq. (7), integer M represents the depth mode number. For fixed values of Θ_B and Θ_S, M is conserved as waveguide parameters in the integral undergo changes. Equation (7) was derived by Weston from a ray viewpoint, and Pierce[15] and Harrison[28] showed that it applies in the case of normal modes. If the phase contributions Θ_B and Θ_S are not constant, but have small variations, M can be considered conserved to leading order in Ref. 28. Furthermore, the connection between rays and modes is noted by Harrison[29] in the coastal wedge environment.

Equation (7) is related to the idealized front model by considering

$$\int_{r_{t1}}^{r_I} \kappa_{r1}(r) dr = \pi m - \frac{1}{2}(\Theta_{r_{t1}} + \Theta_{r_I}). \tag{8}$$

The quantity $r_{t1} = \eta/\mathrm{Re}(k_{r1})$ is the location of the inshore turning point of the radial mode equation[7] in Eq. (4) which is either the zero of $\kappa_{r1}(r)$ for real k_y, or an excellent approximation to the zero for $\mathrm{Im}(k_y) \ll \mathrm{Re}(k_y)$. For $r < r_{t1}$, the radial modes decay exponentially, and for $r_{t1} < r < r_I$ they oscillate. The waveguide integration region lies between the inshore turning point $r = r_{t1}$ and the front $r = r_I$. For the case of WG modes, the phase change Θ_{r_I} at the totally reflective front is 2π. The phase change $\Theta_{r_{t1}}$ at the refractive turning point is $-\pi/2$, which is calculated by examination of connection formulas in the Wentzel-Kramers-Brillouin-Jeffreys approximation.[30]

To evaluate the left side of Eq. (8), note that

$$\kappa_{r1}(r) = k_{r1}\mu'(z), \tag{9}$$

where

$$\mu(z) = \sqrt{z^2 - 1} - \cos^{-1}\left(\frac{1}{z}\right), \quad \mu'(z) = \frac{\sqrt{z^2 - 1}}{z}, \tag{10}$$

and $z = rk_{r1}/\eta$. Integrating both sides of Eq. (9) in z and changing variables from z to r on the left side, Eq. (9) evaluates to

$$\int_{r_{t1}}^{r_I} \kappa_{r1}(r) dr = \eta(\mu(z_1) - \mu(1)) = \eta\mu(z_1), \tag{11}$$

where $z_1 = r_I k_{r1} \eta^{-1}$. Finally, combining Eqs. (8) and (11),

$$\eta\mu(z_1) \sim \pi m - \frac{3\pi}{4}. \tag{12}$$

An estimate for the radial mode number m for given model parameters and k_y can be approximated by solving for m in Eq. (12) and rounding to the nearest integer. Since the mode number m is conserved it follows from Eq. (12) that the quantity $\eta\mu(z_1)$ is invariant to leading order. In the case of TR or Leaky modes, the quantities Θ_{r_I} and $\Theta_{r_{t1}}$ are not constant, but will vary on small scales, as noted in Ref. 28, such that Eq. (12) will still hold.

IV. APPROXIMATION OF THE REFLECTION COEFFICIENT AND DISPERSION RELATION

Parameter dependence was extracted directly from the dispersion relation by Pierce,[31] and in particular variations of bottom slope angle have been treated for influence on donwslope propagation loss by Koch *et al.*[32] The approximate formula Eq. (12) is a key result for determining parameter dependence of acoustic quantities. It was derived by hypothesizing that Weston's integral formula for 2-D waveguides extends to the 3-D feature model of an idealized front. The next two sections describe an alternative approach that puts Eq. (12) on a firm basis, and additionally provides other useful formulas. The dispersion relation relating frequency ω to wavenumber k_y is another conserved quantity in the normal mode formulation. It is computationally convenient to use the dispersion relation in the form $R = 1$ as identified in Ref. 6, where R is the reflection coefficient at the front $r = r_I$. However, consistent with Ref. 7, expressing R as ratios of Hankel functions and their derivatives is computationally convenient and will also allow simpler extractions of asymptotic approximations,

$$R = -\left(k_{r1}\frac{H_\eta^{(1)\prime}(k_{r1}r_I)}{H_\eta^{(1)}(k_{r1}r_I)} - k_{r2}\frac{H_\eta^{(1)\prime}(k_{r2}r_I)}{H_\eta^{(1)}(k_{r2}r_I)}\right) \times \left(k_{r1}\frac{H_\eta^{(2)\prime}(k_{r1}r_I)}{H_\eta^{(2)}(k_{r1}r_I)} - k_{r2}\frac{H_\eta^{(1)\prime}(k_{r2}r_I)}{H_\eta^{(1)}(k_{r2}r_I)}\right)^{-1} \frac{H_\eta^{(1)}(k_{r1}r_I)}{H_\eta^{(2)}(k_{r1}r_I)}. \tag{13}$$

Both orders and arguments of the Hankel functions and derivatives in Eq. (13) are large for the reference values and others of interest. For example, from $\eta = (\pi/\alpha)(n - 1/2)$ with $\alpha = 3°$, η is at least 30, and increases with n. In the arguments, $r_I = 4000$ m, so provided k_y is not close to k_1 or k_2, then $k_{rj}r_I$ will also be large.

The quantities $z_j = r_I k_{rj}\eta^{-1}$ for $j = 1$ and 2 are useful ratios. Typically for reference parameters and for leaky modes, z_j is order $O(10^1)$ for $n = 1$ and no smaller than $O(10^0)$ for other n values (order of magnitude specified using the definition in Ref. 33). Consequently, asymptotic approximations for large order and large argument Hankel and Bessel functions are appropriate for approximating the ratios of Hankel functions in Eq. (13). One of these approximations is[34]

$$\frac{H_\eta^{(1)\prime}(\eta z_j)}{H_\eta^{(1)}(\eta z_j)} \sim -\frac{e^{2\pi i/3}}{z_j}\left(\frac{1 - z_j^2}{\zeta_j}\right)^{1/2}\frac{1}{\eta^{1/3}}\frac{\mathrm{Ai}'(e^{2\pi i/3}\eta^{2/3}\zeta_j)}{\mathrm{Ai}(e^{2\pi i/3}\eta^{2/3}\zeta_j)}, \tag{14}$$

where the Ai is the Airy function of the first kind. In Eq. (13), the ratio with type two Hankel functions yields the same as Eq. (14) with the sign of i changed. The quantity ζ_j is defined as a function of z,

$$\frac{2}{3}(-\zeta_j)^{3/2} = \sqrt{z_j^2 - 1} - \cos^{-1}\left(\frac{1}{z_j}\right) = \mu(z_j), \quad \mathrm{Re}(z_j) \geq 1, \tag{15}$$

where the function $\mu(z)$ from Eq. (10) appears. For leaky modes, the wavenumber condition $\mathrm{Re}(k_y) < k_j^*$ ensures that $\mathrm{Re}(z_j) > 1$ for both $j = 1$ and 2. The approximation has turning points at $z_j = 1$, which correspond to $k_y = k_j^*$ from Eq. (6) and to the zeros of Eq. (3) when $r = r_I$. These are inflection points in the radial modes which separate oscillatory from exponential behavior at the front.

A large order approximation to the Airy functions further simplifies Eq. (14) after which the ratios become[35]

$$\frac{H_\eta^{(1)\prime}(\eta z_j)}{H_\eta^{(1)}(\eta z_j)} \sim \frac{\sqrt{1 - z_j^2}}{z_j}, \quad \frac{H_\eta^{(2)\prime}(\eta z_j)}{H_\eta^{(2)}(\eta z_j)} \sim -\frac{\sqrt{1 - z_j^2}}{z_j}, \quad \frac{H_\nu^{(1)}(k_{r1}r_I)}{H_\nu^{(2)}(k_{r1}r_I)} \sim -ie^{i2\eta\mu(z_1)}. \tag{16}$$

Substituting Eq. (16) into Eq. (13) leads to the expression

$$R \sim \left[\frac{\sqrt{z_1^2 - 1} - \sqrt{z_2^2 - 1}}{\sqrt{z_1^2 - 1} + \sqrt{z_2^2 - 1}}\right] e^{i2(\eta\mu(z_1) - \pi/4)}. \tag{17}$$

Applying the approach outlined here for Leaky modes to WG modes produces the same approximation for R in Eq. (17).

V. CONVENIENT FORMULAS FOR PARAMETER DEPENDENCE

Equation (17) gives a much simpler form of the dispersion relation $R = 1$ than Eq. (13), but it remains too complicated to extract convenient expressions for the wavenumber k_y in terms of feature parameters. This section provides expressions for both the real and imaginary parts of the horizontal wavenumber k_y, which confirm the invariance of $\eta\mu(z_1)$ from Eq. (7), and approximate the along-shore modal attenuation. For this section, the dispersion relation will be used as a starting point, but further approximations are required.

Equation (17) is the starting point, along with the property $\mathrm{Im}(k_y) \ll \mathrm{Re}(k_y)$, that is illustrated by Figs. 2(a) in both Refs. 6 and in 7. Specifically, $\mathrm{Im}(k_y)$ is zero for WG modes in this front model and is two or more orders of magnitude smaller than $\mathrm{Re}(k_y)$ for leaky modes. With the notation $k_y = u + iv$, the quantities z_j for small v/u are well approximated by

$$z_j \sim \bar{z}_j - \left(\frac{r_I}{\eta}\right)^2 \frac{uv}{\bar{z}_j}, \tag{18}$$

where $\bar{z}_j = z_j(k_y = u)$. If A_L is the term in square brackets of Eq. (17) for leaky modes ($\bar{z}_2 > 1$), then Eq. (18) can be used to expand A_L in a Taylor series for small v. This leads to an approximation $A_L \sim \bar{A}_L e^{i2\gamma_L}$ for leaky modes, and a corresponding formula $A_{WG} \sim \bar{A}_{WG} e^{2i\gamma_{WG}}$ for WG modes, containing real quantities $\bar{A}_L$, $\bar{A}_{WG}$, γ_L, and γ_{WG}. The expression $\mu(z_1)$ can be treated similarly, so that the small v Taylor series for leaky modes becomes an approximation for Eq. (17),

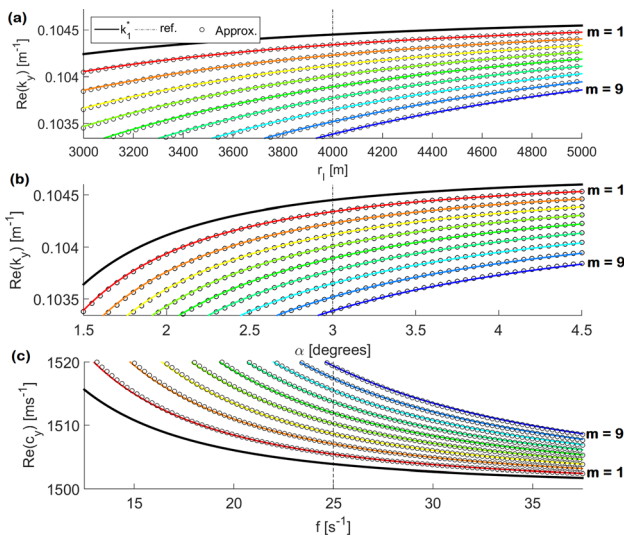

FIG. 2. (Color online) Parameter dependence of WG modes $m = 1$–9, and $n = 1$, comparing approximations from Eqs. (24), (25), and (27) (open circles) to numerically exact curves from Eq. (17) (solid curves). Each curve represents one radial mode number m. Vertical dashed lines are reference parameter values. Thick solid curve is limiting value $k_y = k_1^*$. (a) Curves $k_y(r_I)$, with reference value $r_{I,0} = 4000$ m and r from 3000 to 5000 m. (b) Curves $k_y(\alpha)$, with $\alpha_0 = 3°$, and α from 1.5° to 4.5° (c) Curves $c_y(f)$ with $f_0 = 25$ Hz, and f from 12.5 to 37.5 Hz.

$$R \sim \left[\frac{\sqrt{\bar{z}_1^2-1}-\sqrt{\bar{z}_2^2-1}}{\sqrt{\bar{z}_1^2-1}+\sqrt{\bar{z}_2^2-1}} e^{2\eta u v (r_I/\eta)^2 (\sqrt{\bar{z}_1^2-1}/\bar{z}_1^2)}\right] \times e^{i(2\eta\mu(\bar{z}_1)+2\gamma_L-(\pi/2))} \sim 1. \tag{19}$$

The phase term γ_L from Eq. (19) is calculated as

$$\gamma_L = \tan^{-1}\left(\frac{\left(\frac{r_I}{\eta}\right)^2 uv}{\sqrt{\bar{z}_1^2-1}\sqrt{\bar{z}_2^2-1}}\right) \sim \left(\frac{r_I}{\eta}\right)^2 \frac{uv}{\sqrt{\bar{z}_1^2-1}\sqrt{\bar{z}_2^2-1}} \sim O(v). \tag{20}$$

Therefore the phase γ_L is $O(v)$, and to leading order may be ignored in Eq. (19). Consequently, the requirement that the phase of R in Eq. (19) is an integer multiple of 2π for leaky modes leads to the requirement that $\mu(\bar{z}_1)$ is approximately constant for fixed mode number. This is equivalent to

$$\eta\mu(\bar{z}_1) \sim \eta_0\mu(\bar{z}_{1,0}), \tag{21}$$

where in Eq. (21) $\bar{z}_{1,0}$ uses a known solution to the dispersion relation with wavenumber $k_{y,0} = u_0 + iv_0$.

With an approximation for u from Eq. (21), setting the amplitude in square brackets in Eq. (19) to 1 permits finding an estimate for v. That is, multiply $[\cdot] \sim 1$ by the denominator $(\sqrt{\bar{z}_1^2-1}+\sqrt{\bar{z}_2^2-1})$, collect terms with $\sqrt{\bar{z}_1^2-1}$ and $\sqrt{\bar{z}_2^2-1}$ terms separately and expand in small v to obtain the approximation[35]

$$v \sim \frac{\sqrt{r_I^2(k_2^2-u^2)-\eta^2}}{r_I^2(k_1^2-u^2)-\eta^2}(k_1^2-u^2)\frac{1}{u}. \tag{22}$$

The quantity $\mathrm{Im}(k_y)$ is the modal attenuation coefficient, which describes decay of a radial mode in the along-front direction. Equations (21) and (22) are used in Secs. VI and VII for determining parameter dependence of k_y and other acoustic quantities.

Equation (21) is an approximation that applies to leaky modes. For WG modes an analogous derivation can be performed by calculating A_{WG} and γ_{WG} by carefully accounting for the sizes of $\bar{z}_1$ and $\bar{z}_2$ under the restriction $k_2 < \mathrm{Re}(k_y) < k_1^*$. The WG analogue to Eq. (21) is

$$\eta\mu(\bar{z}_1) + \gamma_{WG} \sim \eta_0\mu(\bar{z}_{1,0}) + \gamma_{WG,0}, \tag{23}$$

where γ_{WG} is bounded by $\pm\pi/2$ as is γ_L in Eq. (20). Because η is large, the γ_{WG} terms in Eq. (23) may be neglected. The final result is that $\mathrm{Re}(k_y)$ for WG and leaky modes is approximated to leading order by Eq. (21). Furthermore, this result is in agreement with Ref. 14, which suggests that $\eta\mu(z_1)$ is invariant. For WG modes, note that in Eq. (22), the quantity $\sqrt{r_I^2(k_1^2-u^2)-\eta^2} = r_I\kappa_{r2,0}(r_I)$. Since no energy oscillates beyond the front for WG modes, the radial wavenumber offshore is zero, so Eq. (22) will evaluate to nearly zero, agreeing with the conditions on WG modes.

VI. FEATURES OF THE PARAMETER DEPENDENCE AND FORMULA ACCURACY

With the basis of Eq. (12) confirmed by asymptotic approximation methods, the invariance of mode number m, and consequently the quantity $\eta\mu(z_1)$, can be used to calculate parameter dependence of the horizontal wavenumber k_y. Given reference parameter values ($r_{I,0} = 4000$ m, $\alpha_0 = 3°$, $f_0 = 25$ Hz, $c_{1,0} = 1500$ ms^{-1}, $c_{2,0} = 1520$ ms^{-1}) suppose a corresponding set of wavenumber solutions $k_{y0,nm}$ to Eq. (13) at the reference values is calculated or estimated for all m and n. Then, Eqs. (21) and (22) can estimate how $\mathrm{Re}(k_y)$ and $\mathrm{Im}(k_y)$ vary with parameter changes from the reference values. From the wavenumber approximations, changes in modal phase speed, attenuation, group speed, and other acoustic quantities with parameter variations can be deduced. For $u = \mathrm{Re}(k_y)$, Eq. (21) leads to the following results that predict how u depends on the parameter in its argument, assuming that the other parameters have their reference values,

$$u(r_I) \sim \sqrt{k_1^2 - \left(\frac{r_{I,0}}{r_I}\right)^2 (k_1^2-u_0^2)}, \tag{24}$$

$$u(f) \sim \sqrt{\left(\frac{2\pi}{c_1}\right)^2 (f^2-f_0^2) + u_0^2}, \tag{25}$$

$$u(c_1) \sim \sqrt{u_0^2 + k_{1,0}^2\left(\frac{c_{1,0}^2}{c_1^2}-1\right)}, \tag{26}$$

$$K(u(\alpha),\alpha) \sim K(u_0(\alpha_0),\alpha_0), \quad K(u(\alpha),\alpha) = \eta(\alpha)\mu(\bar{z}_1(u(\alpha,\alpha))). \tag{27}$$

From Eq. (22) the imaginary component v (and modal attenuation coefficient) is expressed as a function of u and one feature parameter in the form $v \sim v(u(\cdot),\cdot)$.

The parameter variation curves given by Eqs. (24), (25), and (27) are plotted for a selection of radial modes. In Fig. 2 the wavenumbers or phase speeds of WG modes for angular mode number $n = 1$ are shown over intervals of parameter values. Each subfigure shows only curves for WG modes, and the thick black curve represents k_1^* beyond which no inshore standing waves exist. The nine curves correspond to radial mode numbers 1–9, with $m = 1$ closest to the k_1^* cutoff. In all three subfigures, highly accurate computational solutions to Eq. (17) are plotted as solid curves. Solutions from the parameter variation formulas are indicated by open circles, and for all cases they are excellent visual and numerical approximations.

In Fig. 2(a), the front location r_I varies up to 1000 m above and below the reference value 4000 m. As the front moves further from (or nearer to) the shore, $\mathrm{Re}(k_y)$ values are squeezed together (or spread apart). Also in this situation, some modes exit the WG region to become transition modes. Figure 2(b) illustrates the dependence of $\mathrm{Re}(k_y)$ on the bottom slope angle α, varying up to 1.5° above and below the reference value 3°. The overall conclusions for α correspond to those for Fig. 2(a), although the curvatures of

all curves differ in comparison to those in Fig. 2(a). Figure 2(c) plots the dependence of the along-front modal phase speed $c_y = 2\pi f/k_y$ on the source frequency f. The plot of $c_y(f)$ illustrates a different acoustic quantity besides wavenumber, and suggests the straightforward transition between two such plots. Note that all three subfigures show that an increase in the parameter on the abscissa leads to compression of the WG modes into a smaller ordinate interval. Smaller f also shows some WG modes exiting the WG region to become TR and leaky modes. Note that in Figs. 2(a) and 2(b) the horizontal axis is the value k_2 which divides WG and TR modes, while in Fig. 2(c) it is the horizontal line $c_y = c_2 = 1520\ \mathrm{ms}^{-1}$. The parameter c_1 is not illustrated, as the physical limitations on acceptable variation in the sound speed limits the effect of changes in c_1 on $\mathrm{Re}(k_y)$. The relative change in the sound speed across the front is a value change of 1.3%.

Next consider Fig. 3(a), which is analogous to Fig. 2(a) with the important difference that the vertical scale is expanded by a factor of 3. This larger range of wavenumbers includes modes of all three types at $r_I = 4000$ m; three WG modes for the top three curves, TR modes for the middle two, and leaky modes for the three bottom. The boundary between WG and TR modes is the thin black line at k_2, and between TR and leaky is the dashed curve at k_2^*. The parameter dependence equations given by Eqs. (24)–(27) are shown to hold in Sec. V for both WG and leaky modes, but TR modes are not considered. Despite this fact, Eq. (24) is capable of well approximating TR modes and either WG or leaky modes as they change to TR modes by crossing the transition boundaries k_2 or k_2^*. This strikingly smooth evolution of all the exact and approximate curves is shown in Fig. 3(a). By using the correct asymptotic approximations for TR modes as outlined in Ref. 35, the dispersion relation can be expressed as $R \sim A_{TR} e^{i2\gamma_{TR}} \sim 1$, where

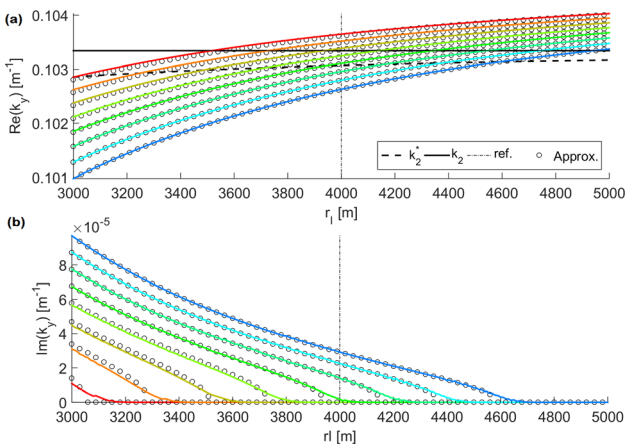

FIG. 3. (Color online) Plots of 8 radial modes $m = 7$–14 for angular mode $n = 1$. Solid curves represent numerically exact dependence on r_I from Eq. (17). The vertical dashed line shows reference value $r_{I,0} = 4000$ m. (a) Open circles show approximations from Eq. (24) for $\mathrm{Re}(k_y)$. Solid horizontal (and curved dashed) line represents $\mathrm{Re}(k_y) = k_2$ (and k_2^*). WG modes occur above k_2, leaky modes below k_2^*, and TR modes between. (b) $\mathrm{Im}(k_y)$ from Eq. (22). Curve behaviors are correlated with expected behavior of the mode types.

$$A_{TR} = \frac{\sqrt{z_1^2 - 1} - \sqrt{1 - z_2^2}\cot\tau}{\sqrt{z_1^2 - 1} + \sqrt{1 - z_2^2}\cot\tau},$$
$$\tau = \frac{\pi}{4} - i\eta\left[\ln\left(\frac{1 + \sqrt{1 - z_2^2}}{z_2}\right) - \sqrt{1 - z_2^2}\right]. \tag{28}$$

Also, z_2 can be approximated as in Eq. (18), with the exception that the $O(v)$ term will be imaginary, since $\bar{z}_2 < 1$. Using an expansion in small $O(v)$, the quantity $\cot\tau$ can be estimated by 1 if $\bar{z}_2 \sim 1$, and i if $\bar{z}_2 < 1$. An expansion for small v in A_{TR} shows that Eq. (21) holds for TR modes as well as WG and leaky modes.[35] This explains why features of Fig. 3(a) are independent of mode type, although the $\mathrm{Im}(k_y)$ approximation for TR modes will differ from Eq. (22) which is designed for leaky modes.

Finally, the parameter dependence of the imaginary part of $\mathrm{Im}(k_y)$ is illustrated for the case of varying front location r_I. Figure 3(b) uses the same modes and r_I values as in Fig. 3(a); with the former's vertical axis having values at least 10^{-3} smaller. It is apparent that $\mathrm{Im}(k_y)$ is well approximated by Eq. (22) over the full spread of r_I values. The approximations even capture well the nonlinear behavior over strongly variable mode transition regimes, between WG to leaky as $\mathrm{Im}(k_y)$ increases from nearly zero. Furthermore, Fig. 3(b) shows that as r_I decreases, $\mathrm{Im}(k_y)$ increases, which implies a higher decay rate in y the alongshore direction.

VII. LOCAL APPROXIMATIONS FOR PARAMETER DEPENDENCE

The formulas in Eqs. (24)–(27) accurately represent wavenumber and modal phase speed changes that result from feature model parameter variations. As indicated by Figs. 2 and 3, they are effective even for relatively large parameter displacements from chosen reference values and across mode type transitions. Because one major goal is to specify sensitivity to variations of parameters in the sharp front feature model, linear approximations for relatively small ("local") parameter changes from reference values are also examined. These provide additional information and insight with lower accuracy for larger displacement from reference parameter variations.

Equation (21) is linearized in terms of quantities Δx that represent small changes of a parameter x from its reference value x_0, for example, $\Delta r_I = r_I - r_{I,0}$,

$$\Delta z_1 \approx \frac{\Delta\alpha}{\alpha_0}\left[\frac{\mu(z_1)}{\mu'(z_1)}\right]_0, \tag{29}$$

where the notation $[\cdot]_0$ denotes evaluation at the reference values $r_{I,0}$, α_0, f_0, and $c_{1,0}$. Expanding the left side of Eq. (29) which involves $u = \mathrm{Re}(k_y)$, leads to

$$[z_1]_0\left(\frac{\Delta r_I}{r_{I,0}} + \frac{\Delta\alpha}{\alpha_0}\right) + \left[\frac{r_I}{\eta}\right]_0\left(\left[\frac{k_1^2}{k_{r1}}\right]_0\frac{\Delta k_1}{[k_1]_0} - \left[\frac{u^2}{k_{r1}}\right]_0\frac{\Delta u}{[u]_0}\right)$$
$$\approx \frac{\Delta\alpha}{\alpha_0}\left[\frac{\mu(z_1)}{\mu'(z_1)}\right]_0. \tag{30}$$

Rearranging Eq. (30) to solve for local changes in u,

$$\left[\sin^2\psi\right]_0 \frac{\Delta u}{[u]_0} \approx \left[\cos^2\psi\right]_0 \frac{\Delta r_I}{r_{I,0}}, \tag{31}$$

$$\left[\sin^2\psi\right]_0 \frac{\Delta u}{[u]_0} \approx \left[\left(\frac{\gamma}{\tan\gamma}\right)\cos^2\psi\right]_0 \frac{\Delta\alpha}{\alpha_0}, \tag{32}$$

$$\left[\sin^2\psi\right]_0 \frac{\Delta u}{[u]_0} \approx -\frac{\Delta c_1}{c_{1,0}}, \tag{33}$$

$$\left[\sin^2\psi\right]_0 \frac{\Delta u}{[u]_0} \approx \frac{\Delta f}{f_0}, \tag{34}$$

where

$$\psi = \tan^{-1}\left(\frac{k_y}{k_{r1}}\right), \quad \gamma = \frac{\pi}{2} - \sin^{-1}\left(\frac{k_\theta}{k_{r1}}\right). \tag{35}$$

Ratios $u/[u]_0$ on the left sides of Eqs. (31)–(34) are changes in u relative to $[u]_0$, and similarly for quantities x/x_0 on the right sides.

Angles ψ and γ can be interpreted physically as illustrated in Fig. 4(a). In Fig. 1(b), the triangular prism sketches the inshore medium wavenumber k_1 as comprised of components $\kappa_1 \equiv \kappa_{r1}(r_I)$ from Eq. (3), k_y, and κ_θ in the radial, along-coast horizontal, and azimuthal directions. The three components satisfy the identity Eq. (5). The quantity $\tan\psi$ is the ratio of the along-shore wavenumber k_y and the inshore vertical plane wavenumber k_{r1}, while $\tan\gamma$ is the ratio of the scaled azimuthal wavenumber κ_θ and the range-dependent inshore radial wavenumber at the front $\kappa_1 = \kappa_{r1}(r_I)$.

Equations (31)–(34) have implications for specifying local parameter sensitivity. In all four equations the relative change in u is scaled by $\left[\sin^2\psi\right]_0 = [u^2/k_1^2]_0$. From the analogous Eq. (31), relative changes in front location r_I are scaled by $\left[\cos^2\psi\right]_0 = [1-(u/k_1)^2]_0$. For physical wavenumbers this quantity is always less than 1 so Eqs. (31) and (34) show that k_y is more sensitive to relative changes in f than to changes in r_I. Furthermore, u will be least sensitive to changes in r_I for short along-coast wavelengths, with $\mathrm{Re}(k_y)$ closest to its largest value of k_1^*. To extract information about slope angle sensitivity from Eq. (32), note that

$$\gamma = \frac{\pi}{2} - \left[\sin^{-1}\frac{\kappa_\theta}{k_{r1}}\right]_0 = \frac{\pi}{2} - \left[\sin^{-1}\frac{1}{z_1}\right]_0. \tag{36}$$

Because solutions of $R=1$, where R is defined as in Eq. (17) must satisfy $\mathrm{Re}(k_y) < k_1^*$, it follows from Eq. (6) and the definition of z_1 that $\mathrm{Re}(z_1) > 1$. As the radial mode number increases, $\mathrm{Re}(k_y)$ decreases and the quantity $1/z_1$ approaches zero, such that γ is between 0 and $\pi/2$. Therefore, $\gamma/\tan\gamma$ in Eq. (32) is between 0 and 1, and Eqs. (31) and (32) show that k_y is less sensitive to relative changes in α than in r_I.

For the frequency f, it is appropriate to specify the sensitivity of the along-front phase speed c_y as in Fig. 2(c). The relative changes in along-front phase speed c_y and frequency f are related by

$$\frac{\Delta C}{[C]_0} \approx -\left[\cot^2\psi\right]_0 \frac{\Delta f}{f_0}, \tag{37}$$

where $C = \mathrm{Re}(c_y) = 2\pi f/u$. By differentiating C with respect to f, substituting the result into Eq. (34), and collecting terms, Eq. (37) can be derived. For other parameters, it is straightforward to show that the local sensitivity of u and C are the same, with the exception of a minus sign.

When linearizations of Eqs. (31)–(34) and Eq. (37) are used to approximate changes to $\mathrm{Re}(k_y)$ based on known (reference) wavenumber solutions, predictions will lose accuracy as parameters increase from the reference values. A maximum variation for Δu is specified next to restrict the sizes of displacements Δx. A choice for a maximum Δu that has a physical interpretation is $\Delta k_m/2$:

$$\Delta k_m = \mathrm{Re}(k_{y,m} - k_{y,m+1}) = u_{m,0} - u_{m+1,0} \approx \frac{2\pi}{\Lambda_{m,m+1}}, \tag{38}$$

where $\Lambda_{m,m+1}$ is the horizontal modal interference length between adjacent radial modes. The quantities Δk_m, $u_{m,0}$, and $u_{m+1,0}$ are illustrated in Fig. 4(b). By requiring

$$\left|\frac{\Delta u_m}{[u_m]_0}\right| < \frac{1}{2}\frac{\Delta k_m}{[u_m]_0} = \frac{\pi}{\Lambda_{m,m+1}}\frac{1}{[u_m]_0}, \tag{39}$$

for a given $u_m = \mathrm{Re}(k_{y,m})$, a direct relation can be made between sensitivity of $\mathrm{Re}(k_y)$ to model parameters and the effect on the horizontal interference length. To obtain an explicit equation for Δk_m, Eq. (12) approximates the difference

$$\mu(z_1)|_{k_{y,m+1}} - \mu(z_1)|_{k_{y,m}} \sim \frac{\pi}{\eta}. \tag{40}$$

The linear approximation $z_1(k_{y,m+1}) = z_1(u_m) + \Delta\bar{z}_{1,m} + O(v)$, where

$$\Delta\bar{z}_{1,m} \approx \left(\frac{r_I}{\eta}\right)^2 \frac{u_m}{\bar{z}_{1,m}} \Delta k_m, \tag{41}$$

relates the small quantities $\Delta\bar{z}_{1,m}$ and Δk_m. Substituting Eq. (41) into Eq. (40) and expanding in Δk_m provides the approximation

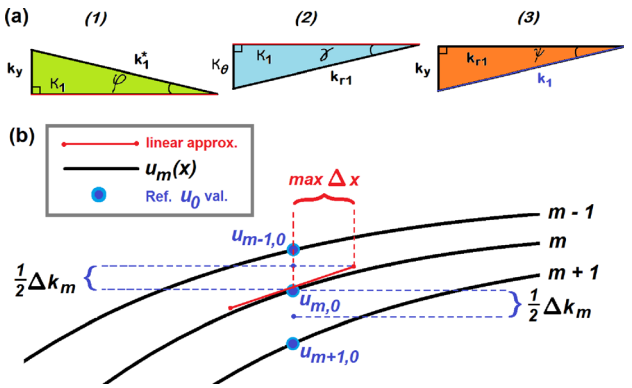

FIG. 4. (Color online) (a) Planar projections of wavenumber components and angles of k_1 corresponding to Fig. 1(b). (b) Schematic illustrating region of validity for local linear approximations. Notation u_m denotes the real part of $k_{y,mn}$, filled (blue) circles on the curves represent real components of k_y dispersion relation solutions for $m-1$, m, and $m+1$ at reference values. Straight solid (red) tangent line represents linear approximation.

$$\Delta k_m \sim \frac{\pi}{\eta}\frac{k_1^2 - u_m^2}{u_m}\frac{1}{\sqrt{\bar{z}_{1,m}^2 - 1}}. \tag{42}$$

For f sensitivity, $\Delta C_m = C_{m+1} - C_m$ is used instead of Δk_m, with the approximation $\Delta C_m \sim C_m(\Delta k_m / k_{y,m})$.

The approximation of Δk_m from Eq. (42), and the restriction on $\Delta u/u_0$ from Eq. (39), along with Eqs. (31)–(34) constrain the maximum relative changes from reference values as follows:

$$\frac{|\Delta r_I|}{r_{I,0}} \leq \left[\frac{\pi}{2\eta}\frac{1}{\sqrt{z_{1,m}^2 - 1}}\right]_0, \tag{43}$$

$$\frac{|\Delta\alpha|}{\alpha_0} \leq \left[\frac{\pi}{2\eta\cos^{-1}(1/z_{1,m})}\right]_0, \tag{44}$$

$$\frac{|\Delta c_1|}{c_{1,0}} \leq \left[\frac{\pi}{2\eta}\frac{k_{r1,m}^2}{k_1^2}\frac{1}{\sqrt{z_{1,m}^2 - 1}}\right]_0, \tag{45}$$

$$\frac{|\Delta f|}{f_0} \leq \left[\frac{\pi}{2\eta}\frac{1}{\sqrt{z_{1,m}^2 - 1}}\right]_0. \tag{46}$$

Note that the relative changes in r_I and f are limited by the same expression. Equations (43)–(46) depend on the mode number under investigation and parameter intervals for their use are readily determined. The largest deviations from reference parameter values to use with local approximations are summarized in Table I for a selection of mode numbers including all three mode types WG, TR, and leaky.

The trends represented by values in Table I are that increasing mode number m requires the parameter intervals for α, r_I, and f to decrease, while the opposite is true for c_1. The WG modes correspond to long-range acoustic propagation along the front, while leaky modes describe near-field behavior. It follows that the far-field behavior in y will be less sensitive to changes in α, r_I, and f compared to the near-field, while the opposite is true for c_1. Overall the linear approximations in Eqs. (31)–(34) show that k_y is most sensitive to changes in f and c_1, and least sensitive to changes in α with r_I sensitivity falling between them. Of course, Eqs. (31)–(34) cannot give comparably accurate predictions of the evolution of k_y that Eqs. (24)–(27) can; but within parameter intervals specified by Eqs. (43)–(46) the linear approximations are reasonably good.

TABLE I. Examples of maximum deviations from reference parameter values for allowed use of local linear approximations, Eqs. (31)–(33) and (37). These deviations are dependent on radial mode number m, angular mode number n, and are the maximum allowed deviation from reference parameter values for a given parameter and mode number. Values are for WG modes $m = 1$ and 5, TR mode $m = 10$, and leaky modes $m = 20$ and 50.

Mode type	Mode #	$\lvert\Delta\alpha\rvert$ deg.	$\lvert\Delta r_I\rvert$ m	$\lvert\Delta f\rvert$ Hz	$\lvert\Delta c_1\rvert$ ms^{-1}
WG	$m = 1$	0.28	328	2.05	0.89
	$m = 5$	0.16	145	0.91	0.86
TR	$m = 10$	0.14	99	0.62	1.04
Leaky	$m = 20$	0.12	64	0.40	1.44
	$m = 50$	0.11	32	0.20	2.71

VIII. SUMMARY AND CONCLUSIONS

Acoustic parameter sensitivity is quantified for a 3-D ocean feature model of an idealized curved sound-speed front over a sloping bottom. The conservation of radial mode number is used to find nonlinear and corresponding linearized approximations of environmental and acoustic parameter variability of horizontal wavenumbers. The nonlinear results are shown to be numerically accurate over quite broad parameter intervals, while the linear results allow easy extraction of detailed parameter sensitivity information for smaller parameter variations. It is concluded that relative changes in model parameters affect $\mathrm{Re}(k_y)$ differently, with $\mathrm{Re}(k_y)$ least sensitive to the bottom slope angle, most sensitive to source frequency and sound speed, and the influence of front location falling between these two. Furthermore, the dependence on mode number illustrates that acoustic behavior in the near-field (in along-shore coordinate y) acoustic behavior is less sensitive to bottom slope angle, front location, and source frequency than is the far field, while the opposite is true for inshore sound speed.

Using the sensitivity and parameter results derived here, estimates could be made of how uncertainty in experimental data influences the results of computational models that include such data in their inputs. Another potential use of these results is identifying effects of environmental variations on acoustic metrics such as modal wavenumber, phase speed, attenuation, and interference length; the relative importance of each environmental variable could be established, and acceptable uncertainty margins could be recommended for experimental data collection. Further research should introduce realism to the idealized model here, to increase applicability of results and to incorporate improved physics, such as a continuously varying front representation and the influences of bottom topography and attenuation processes. Additionally, the effect of parameter changes on other field metrics such as transmission loss could be approximated, and the mode number invariance approach could be applied to other ocean features with fronts, such as nonlinear internal wave ducts.

ACKNOWLEDGMENTS

This work was supported by the Office of Naval Research under grants to Rensselaer Polytechnic Institute (Grant No. N00014-14-1-0372, which is a Special Research Award in Ocean Acoustics for the first author's Ph.D. degree, and also Grant No. N00014-17-1-2370), and to Woods Hole Oceanographic Institution (Grant No. N00014-11-1-0701), which is a Multidisciplinary University Research Initiative.

NOMENCLATURE

Ai	Airy function of the first kind
C	Real component of c_y
c_1	Inshore sound speed
c_2	Offshore sound speed
c_y	Along-front modal phase speed
f	Source frequency
$H_\eta^{(i)}$	Hankel function of the ith kind with order η
Im	Imaginary component
j	Index denoting inshore (1) or offshore (2)
k	Wavenumber in the wedge
k_j	Inshore or offshore wavenumber
k_j^*	(r, y) plane wavenumber, evaluated at the front
k_{rj}	Vertical plane (r, θ) wavenumber
k_y	Horizontal wavenumber
$k_{y,nm}$	Horizontal wavenumber solution of dispersion relation for nth angular mode and mth radial mode
k_θ	Dimensional angular wavenumber
m	Radial mode number
n	Angular mode number
$P(r, \theta, y)$	Acoustic pressure
$\hat{P}(r, \theta, k_y)$	Fourier transform of P
Q_{nm}	Modal weight coefficient
R	Reflection coefficient
Re	Real component
r	Radial coordinate
r_0	Radial location of source
r_I	Radial location of constant curvature front
r_{t1}	Inshore turning point of the radial mode equation
t	Time
u	Real component of k_y
v	Imaginary component of k_y
y	Horizontal coordinate
z_j	Dimensionless ratio of Hankel function argument to Hankel function order, $k_{rj} r_I \eta$
α	Constant bottom slope angle
Δk_m	Real difference between adjacent horizontal wavenumber solutions of the dispersion relation
η_n	Angular wavenumber for nth angular mode
θ	Azimuthal coordinate
θ_0	Azimuthal location of source
κ_1	Inshore radial wavenumber evaluated at the front
κ_{rj}	Radial wavenumber
$\Lambda_{m,m+1}$	Horizontal modal interference length between adjacent radial modes
$\Phi_n(\theta)$	Angular mode function
$\Psi_{nm}(r)$	Radial mode function
ω	Angular source frequency

[1]A. Newhall, K. Von der Heydt, B. Sperry, G. Gawarkiewicz, and J. Lynch, "Preliminary acoustic and oceanographic observations from the Winter Primer Experiment," Woods Hole Oceanographical Institute Technical Report No. WHOI-98-19 (1998).

[2]B. J. Sperry, J. F. Lynch, G. Gawarkiewicz, C.-S. Chiu, and A. Newhall, "Characteristics of acoustic propagation to the Eastern Vertical Line Array Receiver during the summer 1996 New England Shelfbreak PRIMER Experiment," IEEE J. Ocean. Eng. **28**, 729–749 (2003).

[3]D. Tang, J. N. Moum, J. F. Lynch, P. Abbot, R. Chapman, P. H. Dahl, T. F. Duda, G. Gawarkiewicz, S. Glenn, J. A. Goff, H. Graber, J. Kemp, A. Maffei, J. D. Nash, and A. Newhall, "Shallow Water'06: A joint acoustic propagation/nonlinear internal wave physics experiment," Oceanogr. **20**, 156–167 (2008).

[4]J. A. Colosi, T. F. Duda, Y.-T. Lin, J. F. Lynch, A. E. Newhall, and B. D. Cornuelle, "Observations of sound-speed fluctuations on the New Jersey continental shelf in the summer of 2006," J. Acoust. Soc. Am. **131**, 1733–1748 (2012).

[5]G. Jin, J. F. Lynch, C. S. Chiu, and J. H. Miller, "A theoretical and simulation study of acoustic normal mode coupling effects due to the Barents Sea Polar Front, with applications to acoustic tomography and matched-field processing," J. Acoust. Soc. Am. **100**, 193–205 (1996).

[6]Y.-T. Lin and J. F. Lynch, "Analytical study of the horizontal ducting of sound by an oceanic front over a slope," J. Acoust. Soc. Am. **131**, EL1–EL7 (2012).

[7]B. J. DeCourcy, Y.-T. Lin, and W. L. Siegmann, "Approximate formulas and physical interpretations for horizontal acoustic modes in a shelf-slope front model," J. Acoust. Soc. Am. **140**, EL20–EL25 (2016).

[8]Y.-T. Lin, K. G. McMahon, J. F. Lynch, and W. L. Siegmann, "Horizontal ducting of sound by curved nonlinear internal gravity waves in the continental shelf areas," J. Acoust. Soc. Am. **133**, 37–49 (2013).

[9]A. A. Shmelev, J. F. Lynch, and Y.-T. Lin, "Three-dimensional coupled mode analysis of internal-wave acoustic ducts," J. Acoust. Soc. Am. **135**, 2497–2512 (2014).

[10]Y.-M. Jiang, N. R. Chapman, and M. Badiey, "Quantifying the uncertainty of geoacoustic parameter estimates for the New Jersey shelf by inverting air gun data," J. Acoust. Soc. Am. **121**, 1879–1894 (2007).

[11]T. F. Duda, Y.-T. Lin, A. E. Newhall, K. R. Helfrich, W. G. Zhang, M. Badiey, P. F. J. Lermusiaux, J. A. Colosi, and J. F. Lynch, "The 'Integrated Ocean Dynamics and Acoustics' (IODA) hybrid modeling effort," in *Proceedings of the International Conference on Underwater Acoustics* (2014), Vol. 2, pp. 621–628.

[12]T. F. Duda, J. F. Lynch, Y.-T. Lin, W. G. Zhang, K. R. Heilfrich, H. L. Swinney, J. Wilkin, P. F. Lermusiaux, N. C. Makris, D. Y. Yue, M. Badiey, W. L. Siegmann, J. M. Collis, J. A. Colosi, S. M. Jachec, A. E. Newhall, L. Wan, Y. Liu, M. S. Paoletti, Z. Gong, P. J. Haley, L. Zhang, K. Raghukumar, and M. R. Allshouse, "The integrated ocean dynamics and acoustics project," J. Acoust. Soc. Am. **139**, 2026 (2016).

[13]F. B. Jensen, W. A. Kuperman, M. B. Porter, and H. Schmidt, *Computational Ocean Acoustics*, 2nd ed. (Springer, New York, 2011), Chap. 2, Sec. 4.5.2.

[14]D. E. Weston, "Guided propagation in a slowly varying medium," Proc. Phys. Soc. **73**, 365–383 (1959).

[15]A. D. Pierce, "Extension of the method of normal modes to sound propagation in an almost-stratified medium," J. Acoust. Soc. Am. **37**, 19–27 (1965).

[16]D. M. Milder, "Ray and wave invariants for SOFAR channel propagation," J. Acoust. Soc. Am. **46**, 1259–1263 (1969).

[17]L. M. Brekhovskikh and Y. Lysanov, *Fundamentals of Ocean Acoustics* (Springer-Verlag, Berlin, 1973), Chap. 7, Sec. 53.

[18]J. A. Colosi, *Sound Propagation through the Stochastic Ocean* (Cambridge University, New York, 2016), Chap. 8, Sec. 2.1.

[19]A. D. Pierce, "Guided mode disappearance during upslope propagation in variable depth shallow water overlying a fluid bottom," J. Acoust. Soc. Am. **72**, 523–531 (1982).

[20]J. M. Arnold and L. B. Felsen, "Rays and local modes in a wedge-shaped ocean," J. Acoust. Soc. Am. **73**, 1105–1119 (1983).

[21]G. V. Frisk, *Ocean and Seabed Acoustics: A Theory of Wave Propagation* (Prentice-Hall, Englewood Cliffs, NJ, 1994), Appendix B.

[22]J. M. Arnold, "Coupled mode theory of intrinsic modes in a wedge," J. Acoust. Soc. Am. **79**, 31–50 (1986).

[23]M. Hall, "The effects of variations in sound speed on coupling coefficients between acoustic normal modes in shallow water over a sloping bottom," J. Acoust. Soc. Am. **79**, 332–337 (1986).

[24]D. P. Knobles, S. A. Stotts, and R. A. Koch, "Low frequency coupled mode sound propagation over a continental shelf," J. Acoust. Soc. Am. **113**, 781–787 (2003).

[25]C. J. Higham and C. T. Tindle, "Coupled perturbed modes and internal solitary waves," J. Acoust. Soc. Am. **114**, 3119–3124 (2003).

[26]B. Katsnelson, V. Petnikov, and J. Lynch, *Fundamentals of Shallow Water Acoustics* (Springer, New York, 2012), Chap. 9.2, Appendix B.

[27]D. C. Stickler, "Normal-mode program with both the discrete and branch line contributions," J. Acoust. Soc. Am. **57**, 856–861 (1975).

[28]C. H. Harrison, "A relation between multipath group velocity, mode number, and ray cycle distance," J. Acoust. Soc. Am. **132**, 48–55 (2012).
[29]C. H. Harrison, "Ray/mode trajectories and shadows in the horizontal plane by ray invariants," in *Hybrid Formulation of Wave Propagation and Scattering*, edited by L. B. Felsen (Springer, Dordrecht, the Netherlands, 1984), pp. 61–75.
[30]M. H. Holmes, *Introduction to Perturbation Methods* (Springer, New York, 2013), pp. 236–243.
[31]A. D. Pierce, "Parametric solution of the dispersion relation for guided sound propagation in shallow water," J. Acoust. Soc. Am. **39**, 1139–1141 (1966).
[32]R. Koch, S. Rutherford, and S. Payne, "Slope propagation: Mechanisms and parameter sensitivities," J. Acoust. Soc. Am. **74**, 210–218 (1983).
[33]C. C. Lin and L. A. Segel, *Mathematics Applied to Deterministic Problems in the Natural Sciences* (SIAM, Philadelphia, PA, 1988), Chap. 6.3.
[34]M. Abramowitz and I. A. Stegun, *Handbook of Mathematical Functions, Vol. 55 of Applied Mathematics Series* (National Bureau of Standards, Washington, DC, 1964), pp. 368, 448, 449.
[35]B. DeCourcy, "Parameter sensitivity of acoustic propagation in models of curved fronts over uniform slopes," Ph.D. dissertation, Rensselaer Polytechnic Institute, Troy, NY (2017), pp. 44–48, 54.